Biophysical Journal
Article

Biophysical Society

Influence of Pulsed Electric Fields and Mitochondria-Cytoskeleton Interactions on Cell Respiration

Ishan Goswami,[1] Justin B. Perry,[2] Mitchell E. Allen,[2] David A. Brown,[2] Michael R. von Spakovsky,[1] and Scott S. Verbridge[3,*]

[1]Department of Mechanical Engineering, [2]Department of Human Nutrition, Foods, and Exercise, and [3]Department of Biomedical Engineering and Mechanics, Virginia Polytechnic Institute and State University, Blacksburg, Virginia

ABSTRACT Pulsed electric fields with microsecond pulse width (μsPEFs) are used clinically; namely, irreversible electroporation/Nanoknife is used for soft tissue tumor ablation. The μsPEF pulse parameters used in irreversible electroporation (0.5–1 kV/cm, 80–100 pulses, $\sim$100 μs each, 1 Hz frequency) may cause an internal field to develop within the cell because of the disruption of the outer cell membrane and subsequent penetration of the electric field. An internal field may disrupt voltage-sensitive mitochondria, although the research literature has been relatively unclear regarding whether such disruptions occur with μsPEFs. This investigation reports the influence of clinically used μsPEF parameters on mitochondrial respiration in live cells. Using a high-throughput Agilent Seahorse machine, it was observed that μsPEF exposure comprising 80 pulses with amplitudes of 600 or 700 V/cm did not alter mitochondrial respiration in 4T1 cells measured after overnight postexposure recovery. To record alterations in mitochondrial function immediately after μsPEF exposure, high-resolution respirometry was used to measure the electron transport chain state via responses to glutamate-malate and ADP and mitochondrial membrane potential via response to carbonyl cyanide-p-trifluoromethoxyphenylhydrazone. In addition to measuring immediate mitochondrial responses to μsPEF exposure, measurements were also made on cells permeabilized using digitonin and those with compromised cytoskeleton due to actin depolymerization via treatment with the drug latrunculin B. The former treatment was used as a control to tease out the effects of plasma membrane permeabilization, whereas the latter was used to investigate indirect effects on the mitochondria that may occur if μsPEFs impact the cytoskeleton on which the mitochondria are anchored. Based on the results, it was concluded that within the pulse parameters tested, μsPEFs alone do not hinder mitochondrial physiology but can be used to impact the mitochondria upon compromising the actin. Mitochondrial susceptibility to μsPEF after actin depolymerization provides, to our knowledge, a novel avenue for cancer therapeutics.

INTRODUCTION

The mitochondrial network generates metabolites critical for the biosynthetic and catabolic processes inside the cell. Substrates from food are broken down and ultimately channeled to the electron transport chain (ETC) in which a series of reduction/oxidation reactions along the inner mitochondrial membrane are coupled to proton pumping. The resulting proton gradient creates and sustains the mitochondrial membrane potential critical for bioenergetic homeostasis. In mammalian cells, molecular oxygen is the terminal electron acceptor in the ETC. Accordingly, measurement of mitochondrial oxygen consumption provides a reliable measurement of bioenergetic status. Beyond its bioenergetic and biosynthetic functionalities, the mitochondrion is now understood to also act as a signaling organelle. For example, an ETC protein cytochrome C is released by the mitochondrion to initiate cell death. Furthermore, the mitochondrion contains its own DNA, and the signaling between the mitochondrion and the nucleus is now thought to regulate many cellular processes, including those involved in cancer progression. The interested reader is directed to the review in (1). Due to the role of the mitochondrion in cellular processes, particularly in cell death, there is an increasing interest in understanding how applied exogenous transient pulsed electric fields (PEFs) that are used in clinical tumor ablation interact with the mitochondrial network.

A representative clinically used PEF pulse train consists of 80–100 square wave pulses each of width 100 μs delivered via electrodes into the tissue at a frequency of 1 Hz. Note that the clinical modality using PEFs is known as

Submitted January 18, 2018, and accepted for publication April 23, 2018.

*Correspondence: sverb@vt.edu

Editor: Jennifer Curtis.

https://doi.org/10.1016/j.bpj.2018.04.047

irreversible electroporation (IRE) or Nanoknife (2–7). The delivery of energy via PEFs disrupts the plasma membrane, causing loss of cell homeostasis, which can lead to cell death if the cell does not recover from the perturbation. To target organelles such as the mitochondrion, investigators have suggested leveraging the electrical property of the outer cell bilayer membrane. The permittivity of biological lipid cell membranes decreases as the frequency of an exogenous time-oscillating electric field is increased. Similarly, the conductivity of these membranes increases with an increase in frequency of the exogenous oscillating electric field. Thus, when a cell is exposed to an exogenous square wave electric field, the harmonics (or frequency components) dictate the electrical property of the membrane. It has been theoretically and experimentally argued (e.g., (8,9)) that reducing the pulse width of the square wave electric field to the order of a submicrosecond or nanosecond and thereby increasing the number of high-frequency harmonic components can make the outer lipid membrane conductive to the electric field and allow most of the exogenous field to reach the cytoplasmic compartment. An excellent summary of investigations using exogenous fields with nanosecond pulse widths is given in Napotnik et al. (10). As indicated in the research literature, such an approach of increasing higher frequency components of an exogenous square wave electric field has been proposed as a way of targeting the mitochondria with limited impact on the outer cell lipid membrane.

However, contradictory findings have been reported in terms of the impact of nanosecond PEF (nsPEF) on cytochrome C release by mitochondria, with some findings indicating no release and others indicating release. Clearly, it would be beneficial in cancer therapeutics for the latter and not the former to be true. For example, an investigation from 2003 (11) reported exposure of human Jurkat and HL-60 cells to an nsPEF train with varying pulse widths (10–300 ns per pulse) and field strengths (36–150 kV/cm). Note that across all their treatment conditions, an energy density of 1.7 J/cc was delivered. Immediately after exposure, cell fractionation was performed to obtain cytosolic proteins. Immunoblot measurement of cytochrome C revealed an increase in the protein levels with increasing pulse width. The increased level of cytochrome C in the cytosolic compartment was associated directly with the impact of the nsPEF on the mitochondria. A more recent study (12) exposed human T-lymphocytes Jurkat cells and monocytes U937 cells to a pulse train of 100 pulses each with a 10 ns width and 1 Hz frequency. Two field strengths were used: 50 and 150 kV/cm. The expressions of caspase 9 and BAX involved in mitochondria mediated cell death were not detected in either cell line upon exposure to the nsPEF. Immunoblot measurements also confirmed no release of cytochrome C in either case.

Contradictory findings have also been made with regard to the impact of nsPEF on mitochondrial membrane potential, which could indicate whether or not the exogenous field permeabilizes the mitochondrial membrane and thus influences the proton gradient across it, which is critical for ATP production. For example, in Napotnik et al. (13), mitochondrial membrane potential fluorescent dyes rhodamine R123 and tetramethyl rhodamine ethyl ester (TMRE) were used to stain lymphocyte Jurkat cells before nsPEF delivery. After the staining and washing steps, cells were exposed to five or more pulses each with widths of 4 ns delivered at a frequency of 1 kHz with a field magnitude of 100 kV/cm. Fluorescent signals were captured using a microscope, and raw units were compared before and after exposure to the nsPEF. The investigators reported a reduction by 76 and 78% in the raw units of R123 and TMRE, respectively, upon nsPEF exposure. Moreover, there was an induced change of 61 and 12% in the raw units of R123 and TMRE, respectively, in cells treated with protonophore carbonyl cyanide-p-trifluoromethoxyphenylhydrazone (FCCP) as a positive control, which disrupts the mitochondrial membrane potential. Another study using human liver cancer SMMC-7221 cells compared mitochondrial membrane potentials resulting from different microsecond and nanosecond pulse treatments (14). Similar to the previously mentioned study, cells were stained with the R123 dye and washed before exposure to the PEF. The pulse train for the microsecond PEF consisted of an exposure of 8.5 min to 200 V/cm fields and pulse widths of 1.3 μs delivered at a frequency of 50 Hz. The nanosecond pulses had a similar frequency and exposure time with a higher field magnitude (600 V/cm) and a pulse width of 100 ns. Note that this study used an exponentially decaying pulse as opposed to the square pulses used in the other mentioned investigation. As in the previous study, they also report a lowering of the raw fluorescent units in cells treated with either pulse train, although the reduction was steeper in the nanosecond-pulse-treated cells. This was indicative of the mitochondrial membrane potential being perturbed by both the microsecond and nanosecond pulses.

Although the two studies described in the previous paragraph on intact cells provide evidence of the PEF (or more specifically, the nsPEF) impacting the mitochondrial membrane potential, they seem to contradict findings on isolated mitochondria by Estlack et al. (15). In this study, Jurkat and U937 cells were used to isolate mitochondria, which were then exposed to 50 kV/cm and 10–100 pulses each with a 10 ns width delivered at a frequency of 1 Hz. The oxygen consumption was measured using an Agilent Seahorse machine an hour after exposure. The study reported no alterations in mitochondrial respiration with nsPEF exposure, which is indicative of no effect of the nsPEF train used on mitochondrial membrane potential. This contradiction between findings on intact cells and isolated mitochondria leads to the question of whether the differences are due to the complex interactions, both structurally and functionally, that the mitochondria inside the intact cells have with other

cell structures, such as the cell cytoskeleton on which each mitochondrion is anchored. A possibility thus exists that the impact of the nsPEF on the mitochondria is an indirect effect via alterations in some other cellular component. As mentioned earlier, it is hypothesized that the higher frequency harmonics of nsPEFs have limited impact on the outer cell membrane. It, however, cannot be completely ruled out that nsPEFs do indeed change the intracellular ionic concentrations brought about by cell membrane permeabilization. Such alterations in the intracellular environment could also affect mitochondrial respiration.

In contrast, it has been argued that microsecond pulse parameters used in clinical settings do impact mitochondrial membrane potential because of outer cell membrane permeabilization. For example, theoretical predictions by Esser et al. (16) suggest that upon membrane permeabilization, voltage-sensitive organelles such as the mitochondria are exposed to the exogenous PEF. However, the question arises as to which μsPEF amplitudes impact the mitochondrial membrane potential or physiology. A study by Reynaud et al. (17) on isolated rat liver mitochondria suggests that the PEF pulse amplitude for microsecond pulse trains would have to be extremely high to alter mitochondrial physiology. Briefly, isolated rat liver mitochondria were exposed to 5 PEF pulses each with a 100 μs pulse width and a frequency of 0.2 Hz. Increased mitochondrial respiration was indirectly indicated by an increased basal oxygen consumption rate for field strengths up to 2 kV/cm, measured immediately after exposure using Clark-type electrodes. Mitochondrial damage indicated by fusion of the mitochondria was only seen beyond 1 kV/cm. However, exposure of live cell mitochondria to such high fields may not be practical, as we have previously shown in Goswami et al. (18), because a field strength above 700 V/cm with clinically used pulse parameters (width: 100 μs; frequency: 1 Hz; pulses: 80–100) results in very limited cell viability.

Nevertheless, these studies highlight that the influence of nanosecond and microsecond PEFs on mitochondria is still not completely understood. Specifically, a mechanistic understanding needs to be developed on how these PEFs, specifically those used in a clinical setting, impact cell structure and cell signaling. To address this gap in our understanding, the following sections present the results of an investigation of mitochondrial responses in murine triple negative breast cancer 4T1 cells exposed to μsPEFs using clinical parameters previously shown to influence cell signaling (18). The goal is to determine whether mitochondrial perturbations recorded after μsPEF exposure are unique to an electric field effect or whether similar perturbations can be brought about by nonelectrical means. Respecting the structural and functional complexity that exists in a cell, an investigation is also made of whether a disruption of the actin cytoskeleton triggers a higher susceptibility of the mitochondria to μsPEF perturbation.

MATERIALS AND METHODS

Cell line and culture conditions

The triple negative breast cancer murine cell line 4T1 was purchased from the American Type Culture Collection (catalog number: CRL-2539). The 4T1 cells were maintained in a Roswell Park Memorial Institute 1640 culture medium supplemented with 10% (by volume) fetal bovine serum and 1% (by volume) penicillin streptomycin. Cells were sustained in humidified incubators at 37°C and 5% CO_2 and were subcultured at ~80% confluence, whereas a 0.25% trypsin-EDTA solution was used for detachment. All experiments were performed within the first 10 subcultures.

PEF exposure protocol

The protocol was previously reported by Goswami et al. (18). Briefly, following the harvest, the cell pellet was washed with phosphate-buffered saline without calcium or magnesium ($PBS^{-/-}$; Santa Cruz Biotechnology, Santa Cruz, CA) and resuspended in basal growth media with neither serum nor penicillin streptomycin. Approximately 6–8 million cells/cuvette were transferred to 4 mm electroporation cuvettes (Mirus Bio LLC, Madison, WI) in a volume of 600 mL. Each cuvette was placed in a holder through which the cells were exposed to an electric field. The electric voltage required for the μsPEF exposure was generated using an electroporation unit (Harvard Apparatus, Cambridge, MA). Short pulses of 100 μs were delivered at a frequency of 1 Hz. The number of pulses was kept constant at 80. The electric field strength reported in this article was calculated by taking the ratio of electric voltage applied to the distance between the electrodes in the cuvette (4 mm). Two different field strengths were investigated: 600 and 700 V/cm. The viabilities of the 4T1 cells exposed to these field strengths were reported by our earlier study to be 80% (600 V/cm) and 40% (700 V/cm) when evaluated after overnight incubation posttreatment (18). For the untreated controls, cells were transferred to cuvettes and kept in the cuvette for the same duration as the treatment groups without application of an electric field.

Mitochondrial respiration measurements in an Agilent Seahorse XF machine

After exposure to the PEFs, cells (including the untreated controls) were allowed to recover for approximately 30 min in ice while the total cell count was made using a hemocytometer for each sample. Approximately 40,000 cells were seeded in each well of an Agilent Seahorse (Santa Clara, CA) XF24 tissue culture plate and allowed to incubate overnight in a cell culture incubator at 37°C and 5% CO_2. After overnight incubation, samples were washed with assay buffer (Seahorse XF base medium, 10 mM pyruvate, 10 mM glucose, and 2 mM glutamax), after which mitochondrial respiration via oxygen consumption rate (OCR) was measured in the XF24 plate reader following our established protocol (19). Injections of 2 μM ATPase inhibitor oligomycin, 0.5 μM protonophore FCCP, and 1 μM ETC complex III inhibitor antimycin-A were made to measure the mitochondrial response. All concentrations reported are the final concentrations in each well.

Mitochondrial respiration measurements via Oroboros O2k respirometry

Oxygen consumption was determined using our established protocols (20). Immediately after exposure to the PEFs, cells were centrifuged at 200 relative centrifugal force for 5 min. The cell pellet obtained was resuspended in an assay buffer (Buffer Z: 105 mM 2-(N-Morpholino)ethanesulfonic acid potassium salt, 30 mM KCl, 10 mM KH_2PO_4, 5 mM $MgCl_2$-$6H_2O$, 0.5 mg/mL bovine serum albumin, 20 mM creatine, 1 mM EGTA (pH 7.1)

in dH_2O). Two milliliters of the cell suspension containing ~6 million cells was then transferred to the Oroboros O2k respiration chamber. A small volume from the sample was used to determine cell number using a hemocytometer before transferring to the respiration chamber. The O2k respiration chamber is equipped with calibrated oxygen measuring polarographic sensors. The chamber was maintained at 37°C, and the oxygen signals were allowed to stabilize before closing the chamber to the outside air. After closing, the OCR was measured after no injections (basal), 2 mM of malate and 10 mM glutamate (G/M), 5 mM of ADP, and two injections of FCCP with a final chamber concentration of 0.3 μM. All concentrations reported are the final concentrations in each well. For control treatments in which the cells were permeabilized using the chemical digitonin, OCR signals were allowed to stabilize after closing the chamber, after which digitonin (final concentration: 10 μg/mL) was injected. The basal rate was measured once the signals stabilized after digitonin injection. Measurements of the OCR responses to G/M, ADP, and FCCP were as described above.

Quantification of cell permeability using cell permeant calcein

Supernatant from cell culture flasks (growth area: 75 cm^2) was removed, and cells were washed with $PBS^{-/-}$. After the wash, growth media containing 5 μM of the cell permeant calcein acetoxymethyl (AM) (Thermo Fisher Scientific, Waltham, MA) was added to the flask (3 mL/75 cm^2). After a 30 min incubation in a cell culture incubator, the cells were harvested following a standard trypsin-EDTA harvesting procedure. Final samples were placed in a 0.5 mL basal media, which was followed by treatment and immediate centrifugation at 200 relative centrifugal force for 5 min. Samples were then placed on ice, and the supernatant (100 μL) was collected at 10, 15, and 20 min. Fluorescence of calcein was detected in the supernatant using a spectrophotometer (BioRad, Hercules, CA). The raw fluorescent unit (RFU) of controls was monitored such that only those time points at which the RFU of the control did not change considerably were considered for measurements. The permeability was expressed as the fold change of the RFU compared to the controls.

Actin depolymerization using latrunculin B

Supernatant from cell culture flasks (growth area: 75 cm^2) was removed, and cells were washed with $PBS^{-/-}$. After the wash, growth media containing 1 μg/mL latrunculin B (Sigma Aldrich, St. Louis, MO) was added to the flask. After a 10 min incubation in a cell culture incubator, the cells were checked under a microscope to verify morphological changes. The supernatant was discarded, and the cells were washed again with $PBS^{-/-}$. Next, the cells were harvested following a standard trypsin-EDTA harvesting procedure.

Statistical analyses

The software JMP (version 12; SAS Institute, Cary, NC) was used for statistical analyses. Samples were compared using a one-way analysis of variance (ANOVA) followed by a post hoc Tukey's honest significant difference (HSD) test to find means that were significantly different from each other.

RESULTS

The effects of clinically relevant μsPEFs on mitochondrial respiration were evaluated via high-resolution respirometry. Briefly, cells in suspension were exposed to PEFs, after which cells were centrifuged and suspended in an assay buffer. The cell suspension volume of 2 mm was transferred to the oxygraph chamber after which mitochondrial respiration response to the substrates glutamate-malate, ADP, and protonophore FCCP was measured. A comparison of mitochondrial responses between PEF and chemically induced (via digitonin) permeabilizations of the cell membrane was made. In addition, this investigation also probed into the significance of a nexus between the actin cytoskeleton and the mitochondria.

PEFs alone do not influence live cell mitochondrial membrane potential

Cell suspensions were exposed to electric field strengths (i.e., applied voltage/distance between electrodes) of 600 and 700 V/cm. The pulse duration was kept constant at 100 μs (see Fig. S1), which was consistent with clinically used values (21,22). The frequency of the electric fields was 1 Hz, and the number of pulses was 80. These PEF parameters were not only chosen because of their clinical relevance but also because of our previous observation of these field parameters influencing cell signaling in human and murine triple negative breast cancer cells (18).

A preliminary analysis of the mitochondrial respiration of cells exposed to these PEFs was made after allowing overnight incubation. Briefly, cells were exposed to PEFs and then seeded in tissue culture Agilent XF Seahorse well plates. After overnight incubation, mitochondrial activity was measured via OCRs of cells in response to the ATPase synthase inhibitor oligomycin, uncoupling protonophore FCCP, and ETC complex III inhibitor antimycin-A (Fig. 1, *A* and *B*). Two mitochondrial performance indices were calculated: respiratory reserve capacity and ATP production capacity. The respiratory reserve capacity is the difference between the OCRs as a response to uncoupling via FCCP and the basal rate. The protonophore FCCP collapses the mitochondrial membrane potential and is indicative of the maximal respiration that the mitochondria can achieve. Respiratory reserve is a representative measure of the cell's ability to respond to increased metabolic demands. The OCR measured after inhibition of ATPase activity provides the fraction of basal rate involved in ATP production. Thus, the difference between the OCRs measured at the basal condition and after oligomycin injection provides a measure of the ATP production rate capacity of the cells.

The XF metabolic data (Fig. 1 *C*) showed no difference in the respiratory reserve and ATP production capacities between the untreated controls and the cells exposed to 600 V/cm. There was a slight (albeit statistically insignificant) decrease in the respiratory reserve capacity of cells exposed to 700 V/cm. Moreover, the ATP production capacity of cells exposed to 700 V/cm was lower than the untreated control, although it was statistically insignificant. Note that our previous measurements of cellular viabilities after overnight incubation (18) indicate that the live fraction of total cells that survive exposure to PEFs was determined to be ~80 and 40% for 600 and 700 V/cm, respectively. This

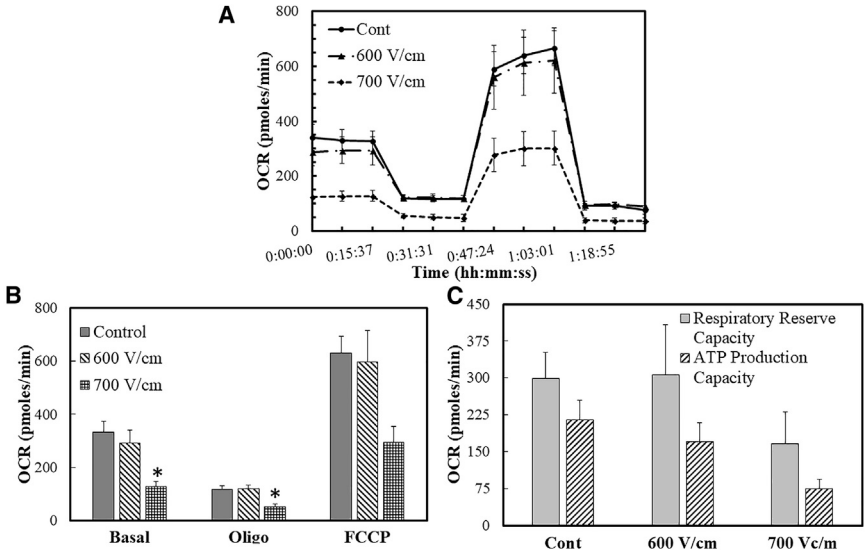

FIGURE 1 The OCR of live cell mitochondria after overnight incubation post-PEF exposure (*A*). The OCR measurements expressed in pmoles/min are summarized in (*B*), and these measurements were used to calculate the respiratory reserve and ATP production capacities (*C*). One-way ANOVA analysis followed by a Tukey's HSD posttest was performed to test for statistical significance. Error bars represent the SE of the mean, and the number of sets per condition is n = 3.

reduction in cell viability is consistent with the reduced absolute respiration rates in cells exposed to 700 V/cm seen in Fig. 1, *B* and *C*.

The XF metabolic data provided no conclusive evidence as to whether mitochondrial physiology is impacted by PEFs because it could be argued that the differences in respiration can be attributed to the fewer live cells in the 700 V/cm group versus the untreated controls. We next proposed that the impact of PEFs on mitochondrial respiration and physiology may only be limited to shorter temporal scales, i.e., immediately after exposure. To test this hypothesis, experiments using high-resolution respirometry were performed on cells exposed to PEFs. Mitochondrial responses to glutamate-malate (G/M), ADP, and protonophore FCCP were measured via the OCR normalized to live cells (pmoles/s-million units; Fig. 2 *A*). The G/M substrate partakes in the complex I activity of the ETC in the mitochondria, whereby an electron is transferred forward through complexes III–IV. The electron flow is used in a series of reduction steps to convert molecular oxygen to water and establish a proton gradient across the mitochondrial membrane. The mitochondrial membrane potential is largely dependent on this proton gradient, and the proton gradient provides the free energy for the ATPase "turbines" (complex V) to phosphorylate ADP to the energy currency ATP. The responses to G/M and ADP thus provide a performance index of the ETC, whereas the disruption of the proton gradient via FCCP collapses the mitochondrial membrane potential.

A representative respirometry plot is shown in Fig. 2 *A*. The initial equilibrated signal of the cell OCR was recorded as the basal rate. Respiration rates of the cells were allowed

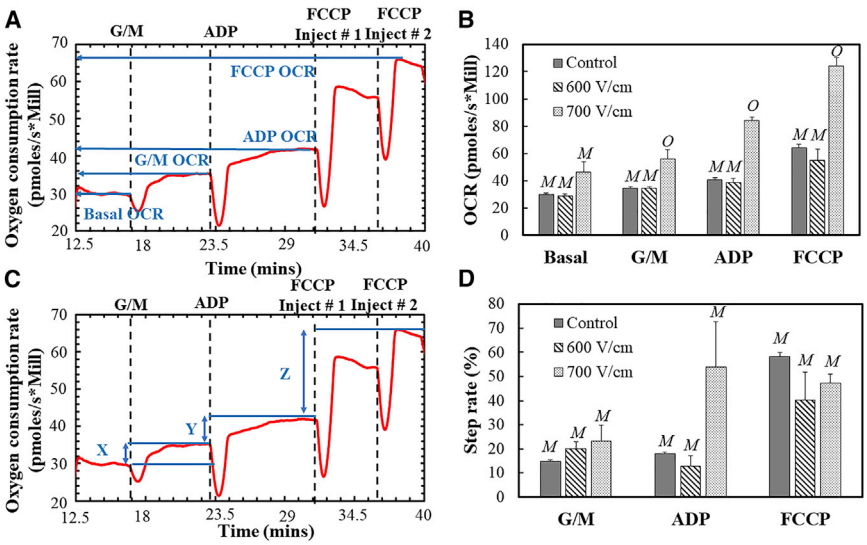

FIGURE 2 Representative oxygen consumption traces are shown in (*A*) and (*C*) as references for (*B*) and (*D*), respectively. The mitochondrial response to glutamate-malate (G/M), ADP, and FCCP was measured via oxygen consumption rates per million cells, as shown in (*B*). Another method of analysis is provided in terms of step heights of the metabolic profile in (*C*). Error bars represent the SE of the mean, and the number of sets per condition is n = 3. Statistically nondistinct conditions were grouped by letter (e.g., M vs. O) for each substrate response to illustrate significant differences as determined by a one-way ANOVA followed by a Tukey's HSD posttest. Note that the dips seen in the respirometry measurements (*A* and *C*) are due to disturbances created by the injections. To see this figure in color, go online.

to stabilize after each injection of substrate/protonophore before making further injections. Two serial injections of FCCP were made, and the highest response was recorded. Normalization of the OCR with live cells was performed by counting the approximate number of total cells via a hemocytometer and assuming the live fraction of the total count (control: 100%; 600 V/cm: 80%; 700 V/cm: 40%) based on independent viability data that we reported with the same cell and pulse conditions (18). Thus, the OCR was normalized and expressed in units of pmoles/s-million cells. Based on the experiments, it was observed that the untreated controls and the cells exposed to 600 V/cm did not have significant differences in mitochondrial responses to G/M, ADP, and FCCP (Fig. 2 *B*). On the other hand, the cells exposed to 700 V/cm had significant differences with both the controls and the 600 V/cm group in all mitochondrial responses. The increased respiration rates after electric field exposure have been previously reported in isolated rat liver mitochondria (17).

A source of error while reporting the normalized OCR is the variability in the total and live cell count. Thus, a normalization technique of the respirometry data independent of the live cell number was deemed useful in countering this variability. Moreover, the OCR after injection of a substrate/protonophore is dependent on the previous OCR step increments. To address these issues, a mathematical expression independent of the number of cells was used to isolate the individual step increments after each substrate injection. This step rate is defined as follows:

$$Step\ rate_i = \frac{OCR_i - OCR_{i-1}}{OCR_{i-1}} \times 100. \qquad (1)$$

In this expression, the subscript "i" denotes a substrate (e.g., ADP) and "$i-1$" denotes the substrate used before "i" (*e.g.*, $i-1$ for ADP is G/M). Thus, graphically the G/M step rate is the height X (Fig. 2 *C*) divided by the basal OCR (Fig. 2 *A*) for the sample. Similarly, the ADP step rate is the height Y divided by the G/M OCR, and the FCCP step rate is the height Z divided by the ADP OCR. These fractions are expressed as percentages in Fig. 2 *D*. Moreover, the ratio in Eq. 1 makes it independent of the number of live cells/mitochondrial mass in the sample. Based on this performance index, it is observed that the PEFs at 700 V/cm induce higher step increments in the G/M and ADP response, although these are not statistically significant from the untreated controls (Fig. 2 *D*). Note that the individual recorded step-rate data for the ADP response in cells exposed to 700 V/cm were higher (31.9, 38.5, 91.2) than that for the controls (19.5, 17.4, 17.1) but possessed high variability because of which a strict statistical analysis would deem the two groups no different from each other. There are lower step increments in the FCCP response in both treatment conditions (600 and 700 V/cm), but again, they are not statistically significant. A lower step increment could indicate the depolarization of the mitochondrial membrane. Thus, based on the data and within the range of microsecond PEF pulse parameters used, the mitochondrial membrane potential and physiology are not significantly altered.

Chemical permeabilization of outer cell membrane leads to altered mitochondrial respiration

Higher step rates for the G/M and ADP injections were recorded for cells exposed to the 700 V/cm PEF (Fig. 2). A possibility exists that electric fields that develop in the cytoplasmic cellular compartment because of permeabilization of the plasma membrane (16) perturb the functioning of the voltage-sensitive ETC. In addition, previous literature (23,24) has reported increased ATP production in an isolated mitochondrion and bacterium when exposed to electric fields similar to those used in this study. However, an alternative explanation is perhaps that the permeabilization of the plasma membrane enhances transmembrane substrate transport to the organelles.

To clarify this issue, we quantified the permeability of cells exposed to PEF pulse parameters within the range used in this study. Briefly, cells were loaded with the cell permeant dye calcein AM. The cell permeant dye is not fluorescent but is cleaved to release fluorescent cell impermeant calcein upon internalization. After a 30 min incubation in a cell culture incubator followed by removal of any residual dye via wash steps with PBS, cells were harvested using trypsin-EDTA solution and exposed to PEFs, as detailed in Materials and Methods. The stained cell sample was then centrifuged, and a pellet was obtained (Fig. S2). A volume of 100 μL was drawn from the supernatant at 10, 15, and 20 min, and the fluorescence was read using a spectrophotometer to measure levels of calcein. Fluorescence units were then normalized to untreated controls for a fold change in RFU. Because the cell impermeant calcein molecule is expected to leak out of permeabilized cells faster than out of the untreated controls, the fold change provides a semiquantitative measure of cell permeability. A similar approach to measure cell permeability is reported by Neri et al. (25). Note that although calcein AM is typically used to measure cell viability, in this investigation (as is done in (25)), it is only used to measure cell permeability. Based on the method described, the RFU fold changes in PEF samples were $\sim$2 for 600 V/cm and $\sim$2.5 for 700 V/cm (Fig. S2).

Next, digitonin detergent (Promega Corporation, Madison, WI) was used to permeabilize the cells and measure the mitochondrial response to the same substrates used for the PEF treatment group. Briefly, cells were placed in the oxygraph chamber, and basal rates were allowed to equilibrate. After equilibration, digitonin was injected to a final concentration of 10 μg/mL. Again, the signal was allowed to equilibrate, after which G/M, ADP, and FCCP were

injected as in the case with the PEF treatment groups. Because the digitonin stock is supplied in a dimethyl sulfoxide (DMSO) solvent, an equal volume (1 μL; final concentration 7 mM) of DMSO (Sigma Aldrich) was also injected to measure changes due to the vehicle of the detergent. Note that the permeabilization due to the digitonin dosage was measured to be ~2 times higher than that of the untreated controls using the same approach as described above, i.e., the permeabilization was comparable to that observed for the PEF-treated samples during the period of the calcein release measurements.

Respirometry measurements were then carried out and are summarized in Fig. 3. The plots illustrate OCR and step-rate measurements for untreated cells (control) and cells exposed to DMSO and digitonin. The OCR measurements reveal that the digitonin significantly reduced the basal rates in cells (Fig. 3 *A*) when compared to the control and DMSO population. Upon examining the step rates (Fig. 3 *B*), the chemical permeabilization induces a higher G/M response, which leads to an insignificant difference in the OCRs between the controls and the digitonin-treated groups (Fig. 3 *A*). The digitonin-permeabilized cells have higher ADP responses when compared to the other two populations (Fig. 3, *A* and *B*). A lower recovery was recorded, as seen in the step-rate data, for the chemically permeabilized cells when perturbed with FCCP (Fig. 3 *B*). Thus, permeabilization via a nonelectrical means also leads to increased responses to the substrates and a reduced response with FCCP injection. An important distinction, however, is the opposite directionality of the alteration in basal rates with the electrical and nonelectrical permeabilization and the much more pronounced G/M and ADP responses with the digitonin permeabilization when the step-rate data are compared.

Actin cytoskeleton and the mitochondrial nexus could dictate mitochondrial response to PEFs

The conflicting findings on the effects of PEFs on mitochondrial physiology in experiments with intact cells versus isolated mitochondria leads to the question of whether there are indirect secondary effects on the mitochondria due to alterations in other cellular structures. The mitochondria are anchored onto the cell cytoskeleton in specialized cytoplasmic domains that allow them to partake in regulatory and energetic processes. For example, mitochondrial positioning in microdomains inside the cytoplasm allows calcium dependent mechanosensing in cardiac cells. For a review, the reader is directed to Schönleitner et al. (26). Aberrations in the localization are implicated in disease. Thus, we next explored the possibility of alterations in the mitochondrial membrane potential with PEFs after chemical alteration of the cytoskeleton. Recent reports (27,28) have demonstrated that PEFs with high-magnitude electric field strengths (19–30 kV/cm; pulse width: order of nanaseconds; number of pulses: 1–4) cause structural damage to the cytoskeleton, including depolymerization of the actin structures (28). We therefore hypothesized that an alteration in mitochondrial function could be achieved with relatively low field strength PEFs (~700 V/cm) after pretreating the cells with an actin depolymerizing agent.

To test this hypothesis, the cells were treated with latrunculin B (LanB) to depolymerize the actin cytoskeleton. The LanB forms a complex with the globular (G)-actin monomer and prevents the polymerization to filamentous (F)-actin (29). Briefly, cells were treated with 1 μg/mL LanB for 10 min. Fixed staining of the cells with the Alexa Fluor Phalloidin conjugate (Thermo Fisher Scientific) for F-actin and the nuclear dye 4',6'-diamidino-2-phenylindole dihydrocholoride (Sigma Aldrich) demonstrated that the dosage of LanB for 10 min was sufficient to compromise the F-actin structures of the 4T1 cells (Fig. 4 *A*). After incubation with LanB, cells were washed with $PBS^{-/-}$ to make sure that no residual drug remained. Cells were then harvested and exposed to a PEF at 700 V/cm, immediately after which respirometry measurements were made, as described in the previous sections. Note that an applied field of 700 V/cm does not imply an equivalent electric dosage between those treated with LanB and those that were not. Furthermore, the cell size directly impacts the influence of the electric field on the plasma membrane (18,30), and therefore, cell size measurements were made. Both untreated controls and LanB-treated cells had a comparable mean diameter. A probability density function of the sizes is provided for reference in Fig. S3. However, one cannot rule out the impact that LanB may have on other lipid reorganization events that may impact the electric field sensed by the cell across the membrane. Because the LanB stock

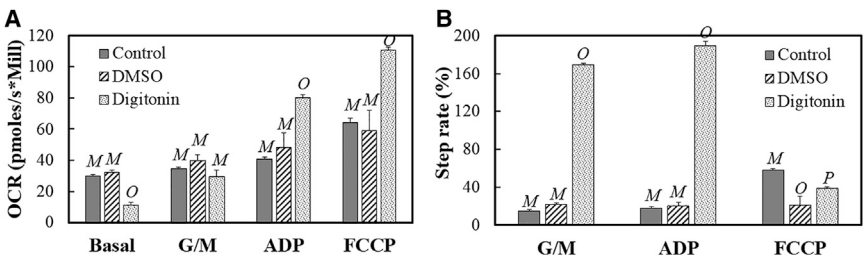

FIGURE 3 The OCR (*A*) and step-rate (*B*) responses to different substrates are shown for cells without any treatment (control) and cells treated with DMSO and digitonin, respectively. Error bars are for the SE of the mean, and n = 3 for the control and DMSO groups, whereas n = 4 for the digitonin group. Statistically nondistinct conditions were grouped by letter (e.g., M vs. O vs. P) for each substrate response to illustrate significant differences as determined by a one-way ANOVA followed by a Tukey's HSD posttest.

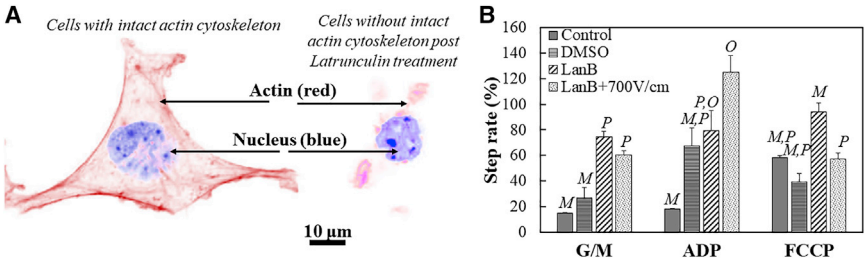

FIGURE 4 Treatment with latrunculin B compromises the actin cytoskeleton, as shown in the fixed cell staining image (*A*) of the actin (*red*) and the nucleus (*blue*). A 10 μm scale bar is shown. Shown in (*B*) are the step-rate data for cells with no treatment (control), those treated with the LanB vehicle DMSO, those treated with LanB, and those with PEF exposure post-LanB treatment. The error bars represent the SE of the mean, and the sample size per set is n = 3 for all except the LanB + 700 V/cm (n = 4) treatment. Treatment conditions connected by different letters (M, O, and P) within each substrate response are statistically different, as determined by a one-way ANOVA followed by a Tukey's HSD posttest. To see this figure in color, go online.

was prepared in DMSO solvent, respirometry was performed on cells incubated with a volume of the vehicle (final concentration 14 mM) equal to that of the LanB. Note that the OCR data normalized to live cells are not provided for this section of the study because of challenges in determining live cell fractions immediately after administration in combinatorial treatments involving PEFs. The challenges are discussed in the section that follows. The step rates obtained from the respirometry measurements are shown in Fig. 4 *B*. The step-rate data of untreated cells (control) and vehicle DMSO are provided for reference.

The step-rate data (Fig. 4 *B*) suggest that treatment with LanB leads to an increased G/M response when compared with untreated controls and cells treated with vehicle DMSO. Upon exposure to a PEF field of 700 V/cm, cells compromised of their actin cytoskeleton via LanB treatment did not significantly differ in their G/M and ADP responses when compared to cells treated with LanB alone. However, actin disruption and PEF exposure reduced the response of cells to FCCP when compared to cells only treated with actin depolymerizing agent LanB. Thus, the step-rate data suggest that relatively low field strength PEFs can impact the mitochondrial membrane potential upon depolymerization of the actin, as seen by the comparison of the FCCP responses between LanB and LanB+700 V/cm groups (Fig. 4 *B*).

DISCUSSION

In this study, murine triple negative breast cancer 4T1 cells were exposed to PEF parameters typically used in a clinical setting. The pulse train used consists of 80–100 pulses each with a 100 μs width applied at a frequency of 1 Hz. Note that this clinical modality is also known as IRE or Nanoknife. The cells were exposed to these μsPEFs, and the mitochondrial states were measured via either an Agilent Seahorse machine or high-resolution respirometry to determine whether these types of microsecond pulses significantly alter mitochondrial physiology.

As a first step, this investigation measured the mitochondrial respiration in cells exposed to 80 μsPEF pulses with amplitudes of 600 and 700 V/cm and incubated overnight. The rationale of choosing these field strengths is twofold. First, there is an immediate severe loss of viability of 4T1 cells at field strengths above 700 V/cm. Thus, an understanding about mitochondrial alterations is lost at these higher strengths because of the damage experienced by the entire cell. Second, it has recently been demonstrated that at field strengths of 600 and 700 V/cm, the μsPEF pulse train induces cell signaling alterations in both murine and human breast cancer cells toward a less immunosuppressive inflammatory state, as determined by the reduction of thymic stromal lymphopoietin signaling (18). The measurements of mitochondrial respiration after overnight incubation were performed using an Agilent Seahorse machine. Note that it is not necessary for the mitochondrial physiology in surviving cells to remain similar to the controls. For example, Zhang et al. (31) reported mitochondrial hyperpolarization in viable cells 24 h after treatment with a drug. Given that the cells that escape μsPEFs had altered cell signaling as reported by Goswami et al. (18), the objective of this investigation was to determine if alterations in mitochondrial respirations are also observed in cells that survive μsPEFs when compared to untreated controls. The data (Fig. 1) gathered in this investigation suggest that there are no significant alterations in the mitochondrial physiology in the cells that escape or recover from the μsPEF treatment. This finding is in agreement with that reported by Estlack et al. (15), who used an almost identical Seahorse protocol and found no alterations in mitochondrial respiration in Jurkat and U937 cells exposed to nsPEFs and allowed to recover over a period ranging from an hour up to as long as 24 h after exposure. Thus, it may be supposed that the effects of these types of nsPEF and μsPEFs on mitochondrial respiration, if any, are short lived (i.e., below 1 h).

To test whether mitochondrial perturbations exist immediately after μsPEF exposure, the mitochondrial respiration of 4T1 cells was measured in this study promptly after treatment with the aforementioned field strengths using high-resolution respirometry. Cell response to injections of G/M and ADP were made to probe the state of the ETC. The changes in OCR in response to G/M reflect alterations in the complex I activity of the ETC, whereas ADP responses provide a measure of the cell's capacity to produce ATP. A final injection of FCCP was made to measure the maximal mitochondrial respiration. When comparing the responses

of control and treatment groups to FCCP, a lowered response in one implies a smaller proton gradient across the mitochondrial membrane and therefore a lower mitochondrial potential compared to another group. The OCR data are dependent on the mitochondrial mass/number, and thus in this investigation, the OCR is normalized to an estimate of the number of live cells based on independent measurements. To circumvent the artifacts that may be introduced because of this cell number and mitochondrial mass dependence, the data are also presented as step rates, whereby an automatic normalization is made within the sample. Such a step-rate approach is very similar to how data using fluorescent dyes are used to measure mitochondrial membrane potential in which the alteration in membrane potential is measured in terms of changes in the fluorescent units before and after a treatment.

Summary of the respirometry data and a comparison with the literature

In this investigation, the respirometry measurements on cells exposed to μsPEFs show increased basal OCR rates 55% higher (albeit not statistically significant) for a field strength of 700 V/cm when compared to the untreated controls (Fig. 2 *B*). Increases in the normalized OCR data were also observed in the G/M (63%), ADP (107%), and FCCP (93%) responses for the μsPEF-exposed population when compared to the untreated controls ($p < 0.05$). Conversely, whereas the step-rate response changes measured were not statistically significant, the trends were that although the G/M and ADP responses in the μsPEF-treated cells increased when compared to the controls, the FCCP response was 18% lower. To explain these respiration responses, we next considered the enhanced permeabilization of the outer membrane that we independently measured for the 600 and 700 V/cm conditions (Fig. S2). Based on the existing literature, a number of plausible scenarios may be responsible for these response alterations due to outer cell membrane permeabilization. They are discussed below.

A first scenario is that the permeability of the cell's outer membrane promotes an unhindered flow of ions and substrates from the extracellular compartment, thereby leading to an increase in respiration due to both G/M and ADP more easily reaching the mitochondria. To recreate this scenario in our experiments, we used a chemical agent digitonin that specifically permeabilizes the outer cell plasma membrane without affecting the nuclear envelope (32,33). The digitonin-permeabilized cells showed decreased basal rates when compared to the untreated controls (Fig. 3 *A*), which (34) claims may be due to a reduction in the adenine nucleotides, resulting in a nonphosphorylating state of the mitochondria. Because of the lower basal rates initially, the G/M response of the digitonin-permeabilized cells was lower by 14% for the normalized OCR data when compared to the G/M response of the untreated controls. The analysis of step-rate data (Fig. 3 *B*), however, provides a clearer picture, showing an increased respiration (>10-fold compared to the controls) in response to the G/M and ADP injections in the digitonin-permeabilized cells. Although the G/M and ADP responses can be explained due to an unhindered flow of substrates into the cell, the question nonetheless arises as to how the mitochondria may be depolarized, as measured by the FCCP response, because of the permeabilization of the cell's outer membrane. In our study, a significant decrease in FCCP step-rate response was recorded in the digitonin-permeabilized cells when compared to the control, suggesting an impact on the mitochondrial membrane potential. Previous measurements on isolated mitochondria of their electrical properties by Pauly et al. (35) and Schwan (36) show an almost linear dependence of the internal conductivity of the mitochondria on changes in the external ionic concentrations. Of course, this relationship may not be linear in live cell mitochondria. Nonetheless, an alteration in the cytoplasmic ionic concentrations due to the permeabilization of the cell's outer membrane and resulting changes in the electrical properties of the mitochondria would be consistent with the FCCP responses we report.

A second scenario is that exogenous electric fields, which gain access into the cell's interior after outer membrane permeabilization, directly affect the mitochondria, contributing to our observed increases in respiration at 700 V/cm. Based on the existing literature, it is thought that an exogenous electric field can either lead to an increase in ATP production by the mitochondria or lead to an alteration in the mitochondrial physiology (i.e., via mitochondrial membrane permeabilization and/or fusion). In experiments conducted by Hamamoto et al. (23), isolated rat liver mitochondria were exposed to PEFs with pulse widths ranging from 100 μs to 10 ms at intervals of 30 s. Hamamoto et al. reported an increase in ATP synthesis in the mitochondria upon exposure to the PEFs, as measured via esterification of the radioactive inorganic phosphate. Moreover, the production increased with increases in both the pulse number and field strengths (>400 V/cm). In their work, the authors claim that the reason for the increase in ADP to ATP turnover with electric fields is due to the artificially imposed ion gradients across the mitochondrial membrane, thus influencing the membrane potential. In addition, they noted that disruption of the mitochondrial membrane potential via FCCP injection disabled the influence of the electric field in stimulating ATP production. This observation of reduced ATP production in the compromised mitochondria of *Escherichia coli* bacteria exposed to μsPEFs has also been reported elsewhere (24). Therefore, based on this literature, as long as the mitochondrial membrane potential does not decrease because of the presence of the electric field, an increase in ATP turnover is possible.

Yet another scenario is that indirect effects on the mitochondria due to a cell's outer membrane permeabilization may occur via alterations in other cellular structures. The disruption of cell homeostasis due to permeabilization could

lead to cell swelling and as a result stress the cell cytoskeleton. For example, actin disassembly due to outer cell permeabilization and cell swelling was reported by Pakhomov et al. (28) when Chinese hamster ovary K1 cells were exposed to nsPEFs (600 ns pulse widths, 2 Hz frequency, ~20 kV/cm). Two other investigations (27,37) in the literature report actin disassembly in plant cells exposed to nsPEFs. However, these latter reports only mention cell permeabilization and not cell swelling. To explore the direct impact of actin disassembly on mitochondrial respiration, we used the drug LanB to depolymerize the actin cytoskeleton. Once the actin network was compromised, the cells were exposed to μsPEF fields of 700 V/cm. The step-rate data (Fig. 4 *B*) shed light on how low-level fields (i.e., low-level when compared to the ~kV/cm fields used by the studies above) can impact the mitochondrial membrane potential once the actin cytoskeleton on which the mitochondria are anchored is compromised. It is noted that Thompson et al. (38) demonstrated that treatment with latrunculin A altered cell membrane rigidity in Chinese hamster ovary cells, making them more susceptible to nsPEF pulses of 150 kV/cm. However, it is difficult to draw specific conclusions regarding the details of mitochondrial effects from the Thompson et al. data. In contrast, in this investigation, a link is provided between actin dynamics and the susceptibility of the mitochondria to μsPEF using detailed mitochondrial respirometry experiments. Although the specific mechanism remains to be explored in future work, a hypothesis may be derived as to why actin depolymerization may impact mitochondria more when exposed to μsPEF based on the existing literature. Actin filament dynamics play an important role in apoptotic pathways (39), such as anoikis. The proapoptotic protein Bmf can translocate from the myosin V actin motor complex to the mitochondria in the event of activation of anoikis and neutralize the antiapoptotic protein Bcl-2 (40). It has also been demonstrated that activation of the caspase cascade leads to fragmentation of the actin cytoskeleton into 31 kDa fractin and 14 kDa tActin. Transfection of tActin into mammalian cells results in morphological alterations (for example, cell rounding) associated with apoptosis, indicating a role for actin fragmentation in the downstream caspase signaling pathway (41,42). In addition to acting as a substrate for the caspase pathway, actin cytoskeleton dynamics can also initiate caspase signaling via both extrinsic and intrinsic apoptotic pathways. For example, CD95/FasL-mediated apoptosis was shown to be dependent on the interaction between the actin-associated ezrin protein and FasL (43). On the other hand, changes in the actin filament dynamics via point mutations in the yeast actin isoform have been shown to induce the accumulation of reactive oxygen species and mitochondrial membrane depolarization involved in intrinsic apoptotic pathways (44). Alteration in the actin filament dynamics brought about by treatment with the drug family latrunculin and cytochalasin D have been shown to induce the translocation of proapoptotic Bcl-2 proteins to the mitochondria and induce mitochondrial depolarization. In addition, experiments on *Arabidopsis* root hair treated with LanB conducted by Wang et al. (45) reveal that actin disruption leads to an opening of the mitochondrial permeability transition pore, which in turn results in a surge in calcium release by the mitochondria. Calcium imbalance in the cytoplasm can alter mitochondrial physiology. It has also been noted that fragmentation into tActin is thought to induce an apoptotic positive feedback loop via cleavage of the proapoptotic protein Bid (46). The nearly 40% reduction in OCR that we observe in response to FCCP injection in the μsPEF-treated cells (LanB + 700 V/cm; Fig. 4 *B*) when compared to the controls (LanB) would be consistent with mitochondrial membrane potential changes enhanced because of actin disruption. Remarkably, Estlack et al. (12) demonstrated that nsPEFs can modulate extrinsic-mediated apoptotic pathways via the CD95/Fas receptor, although intrinsic pathways involving the mitochondria were unaffected. Thus, there remains a largely unexplored area of actin-mitochondria-cell membrane nexus interactions that may dictate the PEF sensitivity of cancerous cells, providing a promising avenue for future work.

In the context of these three scenarios and keeping in mind that this investigation observed neither a drastic decrease in FCCP response nor a drastic increase in ADP turnover in cells exposed only to μsPEFs (Fig. 2), it may be concluded that mitochondrial membrane potential and physiology are not drastically altered by the μsPEF pulse parameters used here.

Note that the effect of substrates and inhibitors (i.e., G/M, ADP, FCCP, etc.) depends on the sequence in which they are applied in an experimental study. Therefore, the relative changes in mitochondrial membrane potential reported in this study are relative changes between two treatments and not absolute values. Although the effects of the sequence of substrates and inhibitors were not explored here, mechanistic computational models of mitochondrial bioenergetics combined with the results from this investigation can guide the formulation of future hypotheses. One such class of computational frameworks uses thermodynamic flux-force relationships to model the coupled transport of mass and charge across the mitochondrial membrane and thus predict the influence that each flux-force term (for example, the flux of Ca^{2+} across the membrane) can have on the kinetics of mitochondrial membrane potential (47–49). Integration of such models with experimental studies have teased out many interesting facets of the link between mitochondrial bioenergetics and apoptosis. For example, Huber et al. (50) demonstrated that increased glycolysis by cancerous cells generated ATP that supported flux reversal of the ATP synthase, thereby repolarizing the mitochondrial membrane potential even in the presence of the adverse conditions normally associated with cell death (cytochrome C release). Such repolarizations allow the cancerous cells to escape apoptotic events. This highlights the need to

investigate the role of the tumor microenvironment, changes in cellular glycolytic capacity, and different phenotypes of cells on mitochondrial response to μsPEFs.

Our studies provide interesting insight into the bioenergetic responses following two different approaches to acutely permeabilize the plasma membrane (using μsPEF and digitonin). Both methods lead to similar cellular rates of ADP- and FCCP-dependent respiration, with each treatment roughly doubling the OCR rate compared to the respective control (Figs. 2 *B* and 3 *A*). These data suggest that the acute treatment with detergent or PEF is not leading to drastic alterations in mitochondrial membrane potential or ATP-generating capacity by the respiratory chain. These findings are in contrast to our studies after overnight incubation post-PEF exposure, where 700 V/cm tended to decrease (albeit not statistically significantly) mitochondrial energetics. It seems plausible that acute buffering of cellular ATP pools by glycolysis may sustain energetics during the acute stressors (as described in Huber et al. (50)), but this buffering capacity may have been exhausted after overnight incubation. There are also interesting differences in mitochondrial energetics between acute permeabilization and acute μsPEF, notably the large step changes after the addition of G/M and ADP (in digitonin compared to μsPEF). We cannot rule out that paradigm-specific differences in the extent/duration of plasma membrane permeabilization led to a cellular "wash-out" of endogenous cofactors that influenced basal and G/M-mediated respiration, which may explain the variance observed after the detergent treatment. Future studies to further probe these ideas, perhaps in conjunction with studies using computational models (47–49), should advance our understanding of the similarities and differences among these models.

However, an important finding in our investigation with implications for the use of PEFs (or IRE/Nanoknife) in cancer therapeutics is that of the relationship between the actin networks and mitochondrial physiology. This is discussed in the following section.

Implications for cancer therapeutics

The clinical site of PEF (or IRE/Nanoknife) delivery in tissue experiences a heterogeneous field, leading to both lethal and sublethal zones. Whereas lethal zones are defined by complete cell death in the region of high electric field exposure, sublethal zones experiencing low-level electric fields persist around the tumor margin where malignant cells may exist. Moreover, the treatment zone is limited in volume by a tradeoff between the high electric field magnitude required to kill cells ($\sim$1000 V/cm) and the magnitude of fields that may be safely delivered clinically without inducing deleterious side effects, such as muscle contractions. It would, therefore, be highly advantageous to be able to increase the tumor treatment volume and/or induce changes in cell signaling toward an antitumor phenotype within a larger sublethal treatment volume (18). To do so, chemo- or molecular-targeted therapies can be leveraged in conjunction with PEF exposure, as is done in electrochemotherapy (51,52) to target sublethal zones. For example, exposure of three-dimensional spheroids to both PEFs and calcium has been shown to specifically inhibit the growth of tumorous cells rather than healthy fibroblasts (53). Similar pulse parameters as in this investigation have been used to make glioblastoma cells more susceptible upon PEF exposure combined with calcium loading (54). Ivey et al. (55) recently reported that cancerous cells were specifically killed by PEFs over healthy cells upon induction of cell morphological changes brought about via molecular targeting of the EphA2 receptor on human glioblastoma cells. This study suggests that molecular adjuvants targeting the actin cytoskeleton could be used in conjunction with PEFs to induce cellular death even with low-strength electric fields by further perturbing the organelles such as the mitochondria. Whereas high-strength electric fields (60–300 kV/cm) have been known to cause damage to the actin cytoskeleton and DNA fragmentation leading to cell death (56,57), molecular adjuvants such as LanB may enhance the kill zone even at low electric field strengths such as those used in our investigation. However, a mechanistic view must be derived to understand the synergistic effects of actin cytoskeleton disruption and PEFs on mitochondrial respiration and the promotion of cell death.

In this regard, several mechanisms by which LanB and related molecules may induce cell death are relatively well documented. Treatment with LanB in the range from 0.01 to 10 μM for 10 min has been reported to cause DNA fragmentation, leading to programmed cell death in pollen cells when assessed 8 h after treatment (58). In human gastric carcinoma cells, treatment with latrunculin A led to increased caspase-3/7 activity when assessed 24 h after treatment. Treatment of these cells with concentrations between 1 and 10 μM led to cell viabilities in the range of 20–60% (59). Another study on human breast cells found that treatment with latrunculin A led to cleavage of the poly (ADP-ribose) polymerase protein involved in DNA damage repair (60). It would therefore be reasonable to assume that the combination of LanB to disrupt the actin cytoskeleton and PEF exposure would induce a higher cell death rate than would the separate treatments alone.

It is worth noting that there are important remaining open questions for future work. A report by Xiao et al. (61) demonstrated outcomes that at first do not seem clearly reconciled with those that we report here. In their study, Xiao et al. exposed human liver cancer cells, pretreated with an actin-depolymerizing drug cytochalasin B, to nsPEFs (450 ns pulse widths delivered at a frequency of 1 Hz and 8 kV/cm). For their measurements of cell death, Xiao et al. used the fact that cells in the early stages of cell death translocate a protein phosphatidylserine from the inner leaflet of the cell membrane to the outside. This

expression of the protein on the cell outer membrane can be detected via annexin V staining. Surprisingly, Xiao et al. report that cells with disrupted actin networks and exposure to PEFs had a reduced percentage of the population expressing this protein when compared to PEFs alone. The reason for this observation is not understood, although it may be noted that annexin V staining on cells performed immediately after PEF permeabilization may provide false positives because the molecule annexin V may be able to access the interior of the cell because of the cell membrane permeabilization caused by the PEF. The primary reason for cellular death with PEFs is hypothesized to be the loss of homeostasis due to a compromised outer membrane. However, the exact mechanism of cellular death caused by PEFs is still debated (62,63). The potential for reversible permeabilization of cells in which cells recover from the loss of homeostasis due to PEFs also makes it difficult to ascertain live cell populations using simple dyes such as trypan blue immediately after PEF treatment. However, we are hopeful that new cancer therapy insights will result from identifying the specific mechanisms regulating cellular responses to combinatorial treatments such as those we investigate here.

CONCLUSIONS

There is a limited understanding of whether μsPEFs based on the IRE/Nanoknife clinical treatment modality directly impact the cell mitochondrial physiology of the treatment zone. To address this gap in knowledge, this investigation provides measurements of the mitochondrial state via high-resolution respirometry on 4T1 cells exposed to μsPEF pulse trains that are used in clinical settings. In these measurements, the ETC state of the mitochondria is probed via responses to G/M and ADP. Additionally, changes in the mitochondrial membrane potential are inferred via responses to FCCP. It is observed in this study that the impact of μsPEFs on mitochondrial respiration is short ($<$1 h) and temporary. Moreover, it is proposed here that these alterations are primarily due to the permeabilization of the cell's outer (plasma) membrane. Comparison between responses of cells exposed to μsPEFs versus the chemical permeabilization agent digitonin indicates that clinically used μsPEFs do not significantly alter mitochondrial physiology within the pulse parameters tested. However, our finding of the mitochondria's susceptibility to sublethal μsPEFs when the cell's actin cytoskeleton is compromised via the actin depolymerizing agent LanB could provide both mechanistic insights as well as avenues for increasing the IRE/Nanoknife treatment volume in a clinical setting.

SUPPORTING MATERIAL

Three figures are available at http://www.biophysj.org/biophysj/supplemental/S0006-3495(18)30572-1.

AUTHOR CONTRIBUTIONS

I.G. conceived the study design, prepared the cell culture, designed the respirometry experiments, performed the data analysis and interpretation, and wrote the manuscript. J.B.P. designed the O2k experiments and wrote the manuscript. M.E.A. designed the XF Seahorse experiments and wrote the manuscript. D.A.B. performed the data analysis and interpretation and wrote the manuscript. M.R.v.S. conceived the project plan and study design, performed the data analysis and interpretation, and wrote the manuscript. S.S.V. conceived the project plan and study design, performed the data analysis and interpretation, and wrote the manuscript.

ACKNOWLEDGMENTS

I.G. was funded by a Computational Tissue Engineering Fellowship offered by the Virginia Tech Interdisciplinary Graduate Education Program. M.E.A. received a research fellowship from the Translational Obesity Research Program of the Virginia Tech Interdisciplinary Graduate Education Program. This work was supported by the National Cancer Institute of the National Institutes of Health through awards R01CA213423, R01HL123647, and P01CA207206, and by a National Science Foundation CAREER Award (CBET-1652112).

REFERENCES

1. Chandel, N. S. 2014. Mitochondria as signaling organelles. *BMC Biol.* 12:34.
2. Jourabchi, N., K. Beroukhim, …, E. W. Lee. 2014. Irreversible electroporation (NanoKnife) in cancer treatment. *Gastrointest. Interv.* 3:8–18.
3. Martin, R. C., II, S. Agle, …, P. Philips. 2017. Efficacy of preoperative immunonutrition in locally advanced pancreatic cancer undergoing irreversible electroporation (IRE). *Eur. J. Surg. Oncol.* 43:772–779.
4. Scheffer, H. J., L. G. Vroomen, …, M. R. Meijerink. 2015. Colorectal liver metastatic disease: efficacy of irreversible electroporation–a single-arm phase II clinical trial (COLDFIRE-2 trial). *BMC Cancer.* 15:772.
5. Scheffer, H. J., L. G. Vroomen, …, M. R. Meijerink. 2017. Ablation of locally advanced pancreatic cancer with percutaneous irreversible electroporation: results of the phase I/II PANFIRE study. *Radiology.* 282:585–597.
6. Scheltema, M. J., W. van den Bos, …, J. J. de la Rosette. 2016. Focal vs extended ablation in localized prostate cancer with irreversible electroporation; a multi-center randomized controlled trial. *BMC Cancer.* 16:299.
7. Trimmer, C. K., A. Khosla, …, J. A. Cadeddu. 2015. Minimally invasive percutaneous treatment of small renal tumors with irreversible electroporation: a single-center experience. *J. Vasc. Interv. Radiol.* 26: 1465–1471.
8. Schoenbach, K. H., A. Abou-Ghazala, …, S. Beebe. 1997. The effect of pulsed electrical fields on biological cells. *Proceedings of the 11th IEEE International Pulsed Power Conference.* 73–78.
9. Ivey, J. W., E. L. Latouche, …, S. S. Verbridge. 2015. Targeted cellular ablation based on the morphology of malignant cells. *Sci. Rep.* 5:17157.
10. Batista Napotnik, T., M. Reberšek, …, D. Miklavčič. 2016. Effects of high voltage nanosecond electric pulses on eukaryotic cells (in vitro): a systematic review. *Bioelectrochemistry.* 110:1–12.
11. Beebe, S. J., P. M. Fox, …, K. H. Schoenbach. 2003. Nanosecond, high-intensity pulsed electric fields induce apoptosis in human cells. *FASEB J.* 17:1493–1495.
12. Estlack, L. E., C. C. Roth, …, B. L. Ibey. 2014. Nanosecond pulsed electric fields modulate the expression of Fas/CD95 death receptor pathway regulators in U937 and Jurkat Cells. *Apoptosis.* 19:1755–1768.

13. Batista Napotnik, T., Y. H. Wu, …, P. T. Vernier. 2012. Nanosecond electric pulses cause mitochondrial membrane permeabilization in Jurkat cells. *Bioelectromagnetics.* 33:257–264.
14. Mi, Y., C. Yao, …, H. Liu. 2009. Apoptosis induction effects of steep pulsed electric fields (SPEF) on human liver cancer cell SMMC-7721 in vitro. *IEEE Trans. Dielectr. Electr. Insul.* 16:1302–1310.
15. Estlack, L. E., C. C. Roth, …, B. L. Ibey. 2014. Investigation of a direct effect of nanosecond pulse electric fields on mitochondria. *Proc. SPIE.* 8941:1–9.
16. Esser, A. T., K. C. Smith, …, J. C. Weaver. 2010. Mechanisms for the intracellular manipulation of organelles by conventional electroporation. *Biophys. J.* 98:2506–2514.
17. Reynaud, J. A., H. Labbe, …, C. Nicolau. 1989. Electric field-induced fusion of mitochondria. *FEBS Lett.* 247:106–112.
18. Goswami, I., S. Coutermarsh-Ott, …, L. R. Bickford. 2017. Irreversible electroporation inhibits pro-cancer inflammatory signaling in triple negative breast cancer cells. *Bioelectrochemistry.* 113:42–50.
19. Dai, W., E. Cheung, …, R. A. Kloner. 2016. Cardioprotective effects of mitochondria-targeted peptide SBT-20 in two different models of rat ischemia/reperfusion. *Cardiovasc. Drugs Ther.* 30:559–566.
20. Alleman, R. J., A. M. Tsang, …, D. A. Brown. 2016. Exercise-induced protection against reperfusion arrhythmia involves stabilization of mitochondrial energetics. *Am. J. Physiol. Heart Circ. Physiol.* 310: H1360–H1370.
21. Martin, R. C., II, K. McFarland, …, V. Velanovich. 2012. Irreversible electroporation therapy in the management of locally advanced pancreatic adenocarcinoma. *J. Am. Coll. Surg.* 215:361–369.
22. Thompson, G. L., C. Roth, …, B. L. Ibey. 2014. Disruption of the actin cortex contributes to susceptibility of mammalian cells to nanosecond pulsed electric fields. *Bioelectromagnetics.* 35:262–272.
23. Hamamoto, T., K. Ohno, and Y. Kagawa. 1982. Net adenosine triphosphate synthesis driven by an external electric field in rat liver mitochondria. *J. Biochem.* 91:1759–1766.
24. Teissié, J. 1986. Adenosine 5′-triphosphate synthesis in Escherichia coli submitted to a microsecond electric pulse. *Biochemistry.* 25: 368–373.
25. Neri, S., E. Mariani, …, A. Facchini. 2001. Calcein-acetyoxymethyl cytotoxicity assay: standardization of a method allowing additional analyses on recovered effector cells and supernatants. *Clin. Diagn. Lab. Immunol.* 8:1131–1135.
26. Schönleitner, P., U. Schotten, and G. Antoons. 2017. Mechanosensitivity of microdomain calcium signalling in the heart. *Prog. Biophys. Mol. Biol.* 130:288–301.
27. Berghöfer, T., C. Eing, …, P. Nick. 2009. Nanosecond electric pulses trigger actin responses in plant cells. *Biochem. Biophys. Res. Commun.* 387:590–595.
28. Pakhomov, A. G., S. Xiao, …, B. L. Ibey. 2014. Disassembly of actin structures by nanosecond pulsed electric field is a downstream effect of cell swelling. *Bioelectrochemistry.* 100:88–95.
29. Morton, W. M., K. R. Ayscough, and P. J. McLaughlin. 2000. Latrunculin alters the actin-monomer subunit interface to prevent polymerization. *Nat. Cell Biol.* 2:376–378.
30. Schoenbach, K. H., B. Hargrave, …, J. A. White. 2007. Bioelectric effects of intense nanosecond pulses. *Dielectr. Electr. Insul. IEEE Trans. On.* 14:1088–1109.
31. Zhang, X., M. Fryknäs, …, S. Linder. 2014. Induction of mitochondrial dysfunction as a strategy for targeting tumour cells in metabolically compromised microenvironments. *Nat. Commun.* 5:3295.
32. Griffis, E. R., S. Xu, and M. A. Powers. 2003. Nup98 localizes to both nuclear and cytoplasmic sides of the nuclear pore and binds to two distinct nucleoporin subcomplexes. *Mol. Biol. Cell.* 14:600–610.
33. Tissera, H., M. Kodiha, and U. Stochaj. 2010. Nuclear envelopes show cell-type specific sensitivity for the permeabilization with digitonin. *Protoc. Exchange* https://doi.org/10.1038/protex.2010.211.
34. Vercesi, A. E., C. F. Bernardes, …, R. Docampo. 1991. Digitonin permeabilization does not affect mitochondrial function and allows the determination of the mitochondrial membrane potential of Trypanosoma cruzi in situ. *J. Biol. Chem.* 266:14431–14434.
35. Pauly, H., L. Packer, and H. P. Schwan. 1960. Electrical properties of mitochondrial membranes. *J. Biophys. Biochem. Cytol.* 7:589–601.
36. Schwan, H. P. 1959. Alternating current spectroscopy of biological substances. *Proc. IRE.* 47:1841–1855.
37. Hohenberger, P., C. Eing, …, P. Nick. 2011. Plant actin controls membrane permeability. *Biochim. Biophys. Acta.* 1808:2304–2312.
38. Thomson, K. R., W. Cheung, …, A. Haydon. 2011. Investigation of the safety of irreversible electroporation in humans. *J. Vasc. Interv. Radiol.* 22:611–621.
39. Desouza, M., P. W. Gunning, and J. R. Stehn. 2012. The actin cytoskeleton as a sensor and mediator of apoptosis. *Bioarchitecture.* 2:75–87.
40. Puthalakath, H., A. Villunger, …, A. Strasser. 2001. Bmf: a proapoptotic BH3-only protein regulated by interaction with the myosin V actin motor complex, activated by anoikis. *Science.* 293:1829–1832.
41. Mashima, T., M. Naito, …, T. Tsuruo. 1997. Actin cleavage by CPP-32/apopain during the development of apoptosis. *Oncogene.* 14:1007–1012.
42. Mashima, T., M. Naito, and T. Tsuruo. 1999. Caspase-mediated cleavage of cytoskeletal actin plays a positive role in the process of morphological apoptosis. *Oncogene.* 18:2423–2430.
43. Parlato, S., A. M. Giammarioli, …, S. Fais. 2000. CD95 (APO-1/Fas) linkage to the actin cytoskeleton through ezrin in human T lymphocytes: a novel regulatory mechanism of the CD95 apoptotic pathway. *EMBO J.* 19:5123–5134.
44. Gourlay, C. W., L. N. Carpp, …, K. R. Ayscough. 2004. A role for the actin cytoskeleton in cell death and aging in yeast. *J. Cell Biol.* 164:803–809.
45. Wang, Y., Y. Zhu, …, Q. Wang. 2010. Disruption of actin filaments induces mitochondrial Ca2+ release to the cytoplasm and [Ca2+]c changes in Arabidopsis root hairs. *BMC Plant Biol.* 10:53.
46. Slee, E. A., S. A. Keogh, and S. J. Martin. 2000. Cleavage of BID during cytotoxic drug and UV radiation-induced apoptosis occurs downstream of the point of Bcl-2 action and is catalysed by caspase-3: a potential feedback loop for amplification of apoptosis-associated mitochondrial cytochrome c release. *Cell Death Differ.* 7:556–565.
47. Beard, D. A. 2005. A biophysical model of the mitochondrial respiratory system and oxidative phosphorylation. *PLoS Comput. Biol.* 1:e36.
48. Bertram, R., M. Gram Pedersen, …, A. Sherman. 2006. A simplified model for mitochondrial ATP production. *J. Theor. Biol.* 243:575–586.
49. Magnus, G., and J. Keizer. 1997. Minimal model of beta-cell mitochondrial Ca2+ handling. *Am. J. Physiol.* 273:C717–C733.
50. Huber, H. J., H. Dussmann, …, J. H. M. Prehn. 2011. Glucose metabolism determines resistance of cancer cells to bioenergetic crisis after cytochrome-c release. *Mol. Syst. Biol.* 7:470.
51. Kunte, C., V. Letulé, …, J. Odili; InspECT (the International Network for Sharing Practices on Electrochemotherapy). 2017. Electrochemotherapy in the treatment of metastatic malignant melanoma: a prospective cohort study by InspECT. *Br. J. Dermatol.* 176:1475–1485.
52. Plaschke, C. C., G. Bertino, …, J. Gehl. 2017. European Research on Electrochemotherapy in Head and Neck Cancer (EURECA) project: results from the treatment of mucosal cancers. *Eur. J. Cancer.* 87: 172–181.
53. Frandsen, S. K., L. Gibot, …, M.-P. Rols. 2015. Calcium electroporation: evidence for differential effects in normal and malignant cell lines, evaluated in a 3D spheroid model. *PLoS One.* 10:e0144028.
54. Wasson, E. M., J. W. Ivey, …, R. V. Davalos. 2017. The feasibility of enhancing susceptibility of glioblastoma cells to IRE using a calcium adjuvant. *Ann. Biomed. Eng.* 45:2535–2547.
55. Ivey, J. W., E. L. Latouche, …, S. S. Verbridge. 2017. Enhancing irreversible electroporation by manipulating cellular biophysics with a molecular adjuvant. *Biophys. J.* 113:472–480.

56. Stacey, M., J. Stickley, …, S. Buescher. 2003. Differential effects in cells exposed to ultra-short, high intensity electric fields: cell survival, DNA damage, and cell cycle analysis. *Mutat. Res.* 542:65–75.

57. Stacey, M., P. Fox, …, J. Kolb. 2011. Nanosecond pulsed electric field induced cytoskeleton, nuclear membrane and telomere damage adversely impact cell survival. *Bioelectrochemistry.* 82:131–134.

58. Thomas, S. G., S. Huang, …, V. E. Franklin-Tong. 2006. Actin depolymerization is sufficient to induce programmed cell death in self-incompatible pollen. *J. Cell Biol.* 174:221–229.

59. Konishi, H., S. Kikuchi, …, E. Otsuji. 2009. Latrunculin a has a strong anticancer effect in a peritoneal dissemination model of human gastric cancer in mice. *Anticancer Res.* 29:2091–2097.

60. Martin, S. S., and P. Leder. 2001. Human MCF10A mammary epithelial cells undergo apoptosis following actin depolymerization that is independent of attachment and rescued by Bcl-2. *Mol. Cell. Biol.* 21:6529–6536.

61. Xiao, D., L. Tang, …, C. Sun. 2011. Effect of actin cytoskeleton disruption on electric pulse-induced apoptosis and electroporation in tumour cells. *Cell Biol. Int.* 35:99–104.

62. Deipolyi, A. R., A. Golberg, …, R. Oklu. 2014. Irreversible electroporation: evolution of a laboratory technique in interventional oncology. *Diagn. Interv. Radiol.* 20:147–154.

63. Maček-Lebar, A., and D. Miklavčič. 2001. Cell electropermeabilization to small molecules in vitro: control by pulse parameters. *Radiol. Oncol.* 35:193–202.